Open quantum system model of the one-dimensional Burgers equation with tunable shear viscosity

Jeffrey Yepez*
Air Force Research Laboratory, 29 Randolph Road, Hanscom Field, Massachusetts 01731, USA
(Received 22 July 2005; revised manuscript received 1 February 2006; published 23 October 2006)

Presented is an analysis of an open quantum model of the time-dependent evolution of a flow field governed by the nonlinear Burgers equation in one spatial dimension. The quantum model is a system of qubits where there exists a minimum time interval in the time-dependent dynamics. Each temporally discrete unitary quantum-mechanical evolution is followed by state reduction of the quantum state. The mesoscopic behavior of this quantum model is described by a quantum Boltzmann equation with a naturally emergent entropy function and H theorem and the model obeys the detailed balance principle. The macroscopic-scale effective field theory for the quantum model is derived using a perturbative Chapman-Enskog expansion applied to the linearized quantum Boltzmann equation. The entropy function is consistent with the quantum-mechanical collision process and a Fermi-Dirac single-particle distribution function for the occupation probabilities of the qubit's energy eigenstates. Comparisons are presented between analytical predictions and numerical predictions and the agreement is excellent, indicating that the nonlinear Burgers equation with a tunable shear viscosity is the operative macroscopic scale effective field theory.

DOI: 10.1103/PhysRevA.74.042322 PACS number(s): 03.67.Lx, 05.60.Gg, 05.30.Ch, 47.40.Nm

I. INTRODUCTION

The purpose of this paper is to theoretically and numerically analyze the dynamical behavior of a quantum model of the classical nonlinear Burgers equation in one spatial dimension. The quantum model is a particular construction or example of an open quantum system with a minimum time step allowing for interleaved nonunitary measurement and unitary evolution. The measurement steps are dispersed periodically in time and across all the elements of the quantum system. At the microscopic scale, the equation of motion is a quantum-mechanical wave equation with localization. That is, the Schrödinger equation is modified in such a way that long-range quantum coherence is destroyed whereby the physical behavior of the system at the macroscopic scale effectively becomes a nonlinear classical field theory with dissipation, the Burgers equation for shock formation.

The state reduction of a phase-coherent quantum system may either be induced by measurement or be intrinsic to the quantum system's unitary evolution. The subject of the measurement apparatus as an open quantum-mechanical system has been studied as a means for understanding the reduction of a quantum state following observation of the system [1–3]. Alternatively, there have been proposals [4–9] that modify the fundamental quantum theory to include microscopic processes that inherently cause the reduction of the quantum state as a way to naturally give rise to macroscopic-scale dissipative behavior. One approach due to Milburn for modifying the Schrödinger equation is to introduce a minimum time step for the quantum-mechanical evolution where at each time step there is a randomization of the unitary phase generated by the system Hamiltonian [4,5]. The resulting evolution is a sequence of unitary transformations instead of being continuous and this evolution sufficiently describes decoherence in open quantum systems [10]. At "laboratory" time scales much larger than this minimum time step, the evolution appears continuous; the Schrödinger equation is recovered at zeroth order and the decay of coherence in the energy eigenstate basis is recovered at first order. Caves *et al.* have developed models of continual quantum measurements distributed in time [11,12] and have developed a path-integral formulation of a one-dimensional quantum system governed by two rules: (1) unitary evolution between measurements and (2) collapse of the wave function at each measurement.

We begin in Sec. I A by summarizing the dynamical equations of motion of the open quantum system and we do this for three spatial scales. The microscopic scale equation is a Schrödinger wave equation modified to allow for localization. The open quantum system comprises a set of two-level qubits (e.g., spin-$\frac{1}{2}$ nuclei). The Hamiltonian that generates the phase-coherent part of the evolution is engineered in such as way that the quantum system effectively models a kinetic many-particle system. The open quantum system acts as a kind of analog simulator.

Each qubit in the system is assigned a unique position and momentum-space coordinate pair. The moduli squared of the probability amplitude of a qubit's logical $|1\rangle$ state (e.g., expectation value of its excited state) is equated to an element of a "single-particle" distribution associated with the position and momentum-space coordinate of a modeled particle in a many-body system. There can be as many particles in the emulated kinetic system as there are qubits in the quantum system. Let us denote a qubit's quantum state as $|q\rangle=\alpha|0\rangle+\beta|1\rangle$, where $|\alpha|^2+|\beta|^2=1$. We shall refer to the state $|0\rangle$ as the qubit's ground state and the state $|1\rangle$ as the qubit's excited state. If $|\alpha|=0$ and $|\beta|=1$, we say that the qubit encodes the presence of a "particle" of unit mass. If $|\alpha|=1$ and $|\beta|=0$, we say that the qubit encodes a "hole," or the absence of a particle. Hence, we shall sometimes refer to $|\beta|^2$ as an occupation probability. The quantum system dynamics comprises both qubit-qubit interaction and motion of the qubits. Some-

*Electronic address: Jeffrey.Yepez@hanscom.af.mil; URL: http://qubit.plh.af.mil

times the terms qubit and particle are used interchangeably.

Further details about the qubit encoding are given in Sec. II A. For reasons of reducing computational expense when simulating the quantum model, the mesoscopic-scale single-particle distribution is highly resolved in position space but minimally resolved in momentum space. The mesoscopic-scale equation of motion of the effective kinetic many-particle system is a quantum Boltzmann equation that governs the time-dependent behavior of the single-particle distribution function. A derivation of the quantum Boltzmann equation from the modified Schrödinger equation is given in Sec. II B. The quantum Boltzmann equation has an unconventional collision function with a unique analytical form that is derived from the microscopic Hamiltonian that generates the locally coherent quantum-mechanical evolution.

A derivation of the collision function is given in Sec. III A. Since the underlying quantum-mechanical system is locally phase coherent, one can ask if there exists an eigenstate of the unitary evolution operator that has a unity eigenvalue. The quantum evolution is stationary with respect to this particular eigenstate: the probability of occurrence of this eigenstate must be identical before and after the local unitary quantum-mechanical evolution. Equating the analytical expressions for these probabilities allows us to uniquely determine the mesoscopic local equilibria associated with the single-particle probability distribution. This calculation is carried out in Sec. III B and the result is that the equilibrium values of the single-particle probability distribution are parametrized by Fermi-Dirac functions. This is consistent with the fact that two-level qubits, or spin-$\frac{1}{2}$ quantum objects, are used to encode these mesoscopic occupation probabilities. The energy eigenvalue of each qubit within a localized region of space is accordingly shifted. That is, the energy eigenvalues of local qubits are nondegenerate.

In Sec. III C, we linearize the quantum Boltzmann equation about its local equilibria and then use a Chapman-Enskog perturbative expansion to derive the nonlinear macroscopic scale equation of motion as the zeroth-order moment of the single-particle distribution function. The macroscopic equation of motion is effectively a diffusive and convective nonlinear Burgers equation. The consequence of this perturbative expansion is an analytically predictable macroscopic-scale transport coefficient, which in this case is the shear viscosity of the modeled fluid. The freedom we have in choosing our local quantum-mechanical evolution translates into our ability to choose any desired shear viscosity in the model, from inviscid flow all the way up to highly viscous flow. In other words, the rate of dissipation is arbitrarily tunable in the model.

Next, in Sec. IV we analyze the nonequilibrium mesoscopic dynamics from the perspective of entropy considerations. This is a way of understanding the numerical stability of the quantum algorithm. The quantum-mechanical entropy function is introduced in Sec. IV A. By extremizing this entropy function, using a Lagrange multiplier to fix energy conservation, we again obtain the Fermi-Dirac function as the local equilibrium for the qubit excited state's occupation probabilities. In Sec. IV B, we calculate an effective transition matrix, defined at the mesoscopic scale, of the quantum system. The transition matrix recasts the quantum evolution as a Markov process at the mesoscopic scale. In Secs. IV B 2 and IV B 3, we demonstrate that the transition matrix of the modeled kinetic system obeys the principle of detailed balance in its qubit-qubit interactions.

Finally, in Sec. V we present several numerical results obtained from simulating the quantum model on a standard classical computer. Shock front development is readily observed. In Sec. V A, the consistency of the entropy function description of the mesoscopic dynamics is compared with the quantum Boltzmann equation description of the dynamics. The entropy function and quantum Boltzmann equation descriptions are found to be in perfect agreement. The quantum collision function maps incoming local qubit configurations into outgoing qubit configurations with higher entropy in such a way that the trajectory of configurations always follows contours on the entropy surface. The quantum model manifests behavior that at the mesoscopic scale emulates the second law of thermodynamics.

A. Multiscale dynamics descriptions

The open quantum system model numerically predicts the time-dependent solutions of the one-dimensional Burgers equation

$$\partial_t u(x,t) + u\partial_x u(x,t) = \nu\partial_{xx} u(x,t), \tag{1}$$

which is a simplified model of shock formation with flow field $u(x,t)$ and kinematic viscosity ν. From a kinetic theory perspective, (1) is the effective field theory for the macroscopic behavior of a system of qubits governed at the mesoscopic scale by a quantum lattice Boltzmann equation:

$$f_\pm(x \pm c\,\delta t, t+\delta t) = f_\pm(x,t) \pm \Omega(f_+,f_-). \tag{2}$$

$f_\pm(x,t)$ are probability fields for the occupation at position x and at time t of a right-moving qubit (+ direction) and a left moving qubit (− direction). $\Omega(f_+,f_-)$ is a nonlinear collision function for local qubit-qubit interaction. A qubit's local speed is $c \equiv \delta x/\delta t$, where δx and δt are the cell sizes of the space-time lattice.

Equation (2) is a statistical description of the kinetic transport dynamics of the system of qubits on a lattice. It is the effective finite-difference equation for the mesoscopic behavior of the microscopic quantum system where the motion of the qubits and their quantum-mechanical interactions are represented by two unitary operators, a streaming operator $\hat{\mathcal{S}}$ and a collision operator $\hat{\mathcal{C}}$, respectively, according to the quantum lattice gas paradigm [13]. The spatial displacement of $f_\pm$ appearing on the left-hand side (LHS) of (2) derives from the unitary streaming operator $\hat{\mathcal{S}}$. Taylor-expanding $f_\pm(x \pm c\,\delta t, t+\delta t)$ about the space-time point (x,t) gives rise to a parabolic partial differential equation. Hence, (2) can be written in differential point form as $\partial_t f_\pm(x,t) = \hat{\mathcal{L}}_\pm f_\pm(x,t) \pm (1/\delta t)\Omega(f_+,f_-)$, where $\hat{\mathcal{L}}_\pm = \partial_x(\mp c - \mathcal{D}_0\partial_x)$ is a Fokker-Planck operator, c is a constant drift coefficient, and $\mathcal{D}_0 = (1/2)(\delta x^2/\delta t)$ is the diffusion coefficient. Here, the reason the spatial derivatives occur at second order while the temporal derivative occurs at first order is that the diffusive ordering of the fluctuations $\varepsilon \sim \delta x \sim \sqrt{\delta t}$ arises because of the

microscopic random walk motion of the qubits. The form of the nonlinear collision function $\Omega(f_+,f_-)$ on the RHS of (2) is derived from the unitary collision operator $\hat{\mathcal{C}}$ in Sec. III A. In Sec. III B the nonlinear collision function is linearized about the equilibrium occupation probabilities $f_\pm^{\mathrm{eq}}$. Then using a perturbative technique in Sec. V C, corrections to the drift and diffusion coefficients arise from the quantum-mechanical qubit-qubit interactions, particularly nonlinearities appearing in the drift. The result is a nonlinear parabolic partial differential equation for the sum of the occupation probabilities $f_+ + f_-$.

Denoting the microscopic quantum state of the system at time t by $|\Psi(t)\rangle$, the microscopic quantum-mechanical evolution equation is written as follows:

$$|\Psi(t+\delta t)\rangle = \hat{\mathcal{S}}\hat{\mathcal{G}}\hat{\mathcal{C}}|\Psi(t)\rangle. \tag{3}$$

Equation (3) reduces to the Schrödinger wave equation when the operator $\hat{\mathcal{G}}$ is the identity operator. A quantum-mechanical evolution, such as is governed by the Schrödinger wave equation, is both linear and nondissipative. The reason for employing the unconventional operator $\hat{\mathcal{G}}$ is to induce both nonlinearity and dissipation into the effective dynamics. There are various alternatives for the operational form of $\hat{\mathcal{G}}$. As mentioned above, one representational choice for $\hat{\mathcal{G}}$ is the nonunitary process of quantum measurement that effectively erases local phase information contained in the wave function upon its collapse. Another representational choice for $\hat{\mathcal{G}}$ is as a unitary operator that randomly alters the local phase of the wave function. In either case, the result is similar and local in its effect at the space-time point where $\hat{\mathcal{G}}$ is applied: coherent phase information, and entanglement, is lost. It is this essential projective property of the $\hat{\mathcal{G}}$ operator to which we ascribe the nonlinearity and dissipation of the model and to which we refer by using the terms wave function localization or open quantum system.

B. Application to quantum computing

The type of open quantum model treated in this paper may be viewed as a parallel quantum algorithm designed for implementation on a quantum computer with periodic state reduction. Equation (3) comprises a four-step quantum algorithm: (1) initialization step [state preparation of $|\Psi(t)\rangle$], (2) collision step (entanglement of the quantum state by $\hat{\mathcal{C}}$), (3) localization step (long-range decoherence or reduction of the quantum state by $\hat{\mathcal{G}}$), and (4) streaming step (interchange of amplitudes by $\hat{\mathcal{S}}$).

The Hamiltonian $\mathcal{H}$ that generates the unitary quantum evolution in (3), when formally expressed as $e^{i\hat{\mathcal{H}}\delta t/\hbar} \equiv \hat{\mathcal{S}}\hat{\mathcal{C}}$, may be called a quantum lattice-gas Hamiltonian (type-I case). Quantum models of the form given by (3), when $\hat{\mathcal{G}}$ is the identity, are known as quantum lattice-gas algorithms and include models by Riazanov [14], Feynman and Hibbs [15], Jacobson and Schulman [16], Bialynicki-Birula [17], Succi *et al.* [18–21], Meyer [22–26], Boghosian *et al.* [27–29], Yepez and Boghosian [30], and Vahala *et al.* [31–34]. However, for (3) to give rise to a macroscopic dissipative effective field theory, such as (1) with viscous dissipation proportional to the curvature of the flow field, $\hat{\mathcal{G}}$ can be chosen to be a projection operator that commutes with the number operator (type-II case).

Parallel quantum algorithms of this sort for computational physics have been developed to numerically predict time-dependent field solutions of the classical wave equation [13,35], the diffusion equation [36,37], the Navier-Stokes equation [38], the nonlinear Burgers equation [39,40], and the one-dimensional equations for magnetohydrodynamic shocks [41]. Such parallel quantum algorithms do not fully exploit the computational complexity of the underlying quantum computer because of the imposed state reduction. Hence, any quantum-mechanical complexity that provides an algorithmic speedup can only be harnessed locally over a relatively limited spatial region. So long as the spatial localization limits phase coherence to less than a few dozen qubits, implementation of the parallel quantum algorithms is straightforward using present-day classical computers; otherwise these parallel quantum algorithms could only be implemented on type-II quantum computers that may be built some day [42]. The first parallel quantum algorithms for the diffusion and Burgers equations have with success been experimentally tested on quantum-information-processing prototypes of parallel quantum computers, or type-II quantum computers [43], using spatial nuclear magnetic resonance (NMR) spectroscopy on a linear array (in both position-space and momentum space) of segmented ensembles of two-qubit labeled chloroform molecules [44–46]. The experimental implementation details and results from a recent NMR-based quantum-information processing experiment of the open quantum model presented in this paper are discussed in the following paper [46].

II. MODEL CONSTRUCTION

A. Qubit encoding

We consider a quantum system with Q number of qubits used to encode (3). A quantum lattice-gas system with $L = Q/2$ number of nodes is depicted in Fig. 1 where, at the microscopic scale, two qubits $|q_+\rangle$ and $|q_-\rangle$ per node are used to encode the mesoscopic probabilities f_+ and f_- of the qubit excited-state occupations at that node:

$$|q_\pm(x,t)\rangle = \sqrt{1-f_\pm(x,t)}|0\rangle + \sqrt{f_\pm(x,t)}|1\rangle, \tag{4}$$

for $0 \leqslant f_\pm \leqslant 1$, and where $|0\rangle$ and $|1\rangle$ denote the ground state and excited state, respectively, of a qubit. Each qubit in the system is independently set; the on-site ket $|\psi(x,t)\rangle$ is a tensor product over the qubits residing at site x,

$$|\psi(x,t)\rangle = |q_+(x,t)\rangle \otimes |q_-(x,t)\rangle, \tag{5}$$

for all x. At time t, the quantum state of the entire microscopic quantum lattice-gas system in (3) is the tensor product of all the on-site kets:

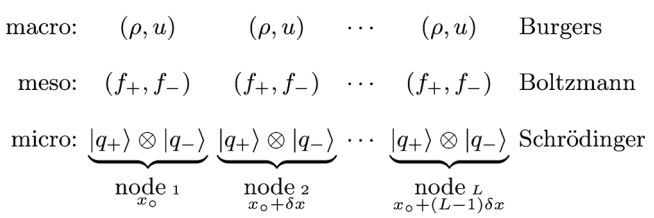

FIG. 1. A type-II quantum lattice gas with L nodes and two qubits per node depicted at three spatial scales. The array is one dimensional with periodic boundary conditions. The coordinate x_0 refers to the location of the first node. The symbol $\otimes$ represents the tensor (or outer) product operation. At the lowest level are microscopic field quantities (i.e., amplitudes of qubit states) governed by the modified Schrödinger equation (3) with a "programmed" Hamiltonian. At the middle level are mesoscopic field quantities (i.e., occupation probabilities $f_\pm$) governed by the quantum Boltzmann equation (2). Finally, at the highest level are macroscopic field quantitites (i.e., ρ or u) governed by the nonlinear Burgers equation (1).

$$|\Psi(t)\rangle = \bigotimes_{j=0}^{L-1} |\psi(x+j\delta x,t)\rangle. \tag{6}$$

Since the qubits can be thought of as containers for encoding the quantum particle occupation probabilities according to (4), the particle number operator is equivalent to the qubit number operator. Let $\hat{n}_\alpha$, where $\alpha=1,\ldots,Q$, denote the qubit number operator for the αth qubit at site x. The occupancy probability of a particle located at the αth qubit at time t is the matrix element

$$f_\alpha(x,t) \equiv \langle\Psi(t)|\hat{n}_\alpha|\Psi(t)\rangle. \tag{7}$$

Because the quantum state (6) is separable over the nodes of the lattice, (7) can be rewritten using the on-site ket at node x:

$$f_\pm(x,t) \equiv \langle\psi(x,t)|\hat{n}_\pm|\psi(x,t)\rangle, \tag{8}$$

where we have assumed the on-site kets are normalized $\langle\psi(x,t)|\psi(x,t)\rangle=1$ for all x, and where $\hat{n}_+\equiv\hat{n}\otimes\mathbf{1}$ and $\hat{n}_-\equiv\mathbf{1}\otimes\hat{n}$ are defined in terms of the singleton number operator $\hat{n}$.

B. Quantum Boltzmann equation

Here we shall derive (2) from (3). The application of $\hat{\mathcal{S}}$ causes the amplitudes associated with the $|q_+\rangle$ qubits to move to the right by δx and the amplitudes of the $|q_-\rangle$ qubits to the left. In particular, say $|\Psi'\rangle=\hat{\mathcal{S}}|\Psi\rangle$ causes the amplitudes of the αth qubit to be transferred to the α'th qubit. Then, by streaming, the occupation probabilities shift so that we must have the equality $f_{\alpha'}=f_\alpha$. By (7), this equality is expressible directly in terms of the operators:

$$\hat{\mathcal{S}}^\dagger\hat{n}_{\alpha'}\hat{\mathcal{S}} = \hat{n}_\alpha. \tag{9}$$

The identity (9) will allow us to derive (2) from (3). We include collisional scattering and write

$$f_{\alpha'} \overset{(7)}{=} \langle\Psi(t+\delta t)|\hat{n}_{\alpha'}|\Psi(t+\delta t)\rangle \tag{10}$$

$$\overset{(3)}{=} \langle\Psi(t)|\hat{\mathcal{C}}^\dagger\hat{\mathcal{G}}^\dagger\hat{\mathcal{S}}^\dagger\hat{n}_{\alpha'}\hat{\mathcal{S}}\hat{\mathcal{G}}\hat{\mathcal{C}}|\Psi(t)\rangle \tag{11}$$

$$\overset{(9)}{=} \langle\Psi(t)|\hat{\mathcal{C}}^\dagger\hat{\mathcal{G}}^\dagger\hat{n}_\alpha\hat{\mathcal{G}}\hat{\mathcal{C}}|\Psi(t)\rangle. \tag{12}$$

Since $\hat{\mathcal{G}}$ commutes with $\hat{n}_\alpha$ for all α, and $\hat{\mathcal{G}}^\dagger\hat{\mathcal{G}}=1$, we have

$$f_{\alpha'} - f_\alpha = \langle\Psi(t)|\hat{\mathcal{C}}^\dagger\hat{n}_\alpha\hat{\mathcal{C}} - \hat{n}_\alpha|\Psi(t)\rangle, \tag{13}$$

where we have subtracted $f_\alpha=\langle\Psi(t)|\hat{n}_\alpha|\Psi(t)\rangle$ from both sides of (13). In the continuum limit, as the lattice resolution becomes infinite ($\delta x\to 0$ and $\delta t\to 0$), the occupation probabilities form a continuous and differentiable field in position space. Defining its total time derivative as $(f_{\alpha'}-f_\alpha)/\delta t$, we obtain the general form of (2):

$$\frac{df_\alpha}{dt} = \frac{1}{\delta t}\langle\Psi(t)|\hat{\mathcal{C}}^\dagger\hat{n}_\alpha\hat{\mathcal{C}} - \hat{n}_\alpha|\Psi(t)\rangle. \tag{14}$$

Because of the diffusive ordering of the temporal and spatial fluctuations of f_α, we expand the LHS to first order in time and second order in space. Furthermore, since the collisions are separable over the nodes of the lattice, $\hat{\mathcal{C}}=\otimes_{j=0}^{L-1}\hat{U}$, where $\hat{U}$ is the on-site collision operator, we recover (2) where the type-II collision function is

$$\Omega[\psi(x,t)] = \langle\psi(x,t)|\hat{U}^\dagger\hat{n}_\pm\hat{U} - \hat{n}_\pm|\psi(x,t)\rangle. \tag{15}$$

C. Macroscopic field assignment

The mesoscopic probabilities $f_\pm$ in turn are used to calculate the macroscopic variables using the Chapman-Enskog perturbative expansion given in Sec. III C. The number density field $\rho(x,t)$ is

$$\rho(x,t) \equiv f_+(x,t) + f_-(x,t), \tag{16}$$

and the flow field $u(x,t)$ in (1) is

$$u(x,t) \equiv c[f_+(x,t) + f_-(x,t) - 1], \tag{17}$$

where the propagation speed of the qubits is the ratio of the lattice cell size to the time step interval, $c=\delta x/\delta t$, as is characteristic of lattice-gas models.[1]

D. Summary of the four-step quantum algorithm

Equation (3) is encapsulated in the following four steps.

(1) Initialization step. The state of the quantum lattice gas is set as specified in Fig. 1, where $|q_\pm(x,t)\rangle=\sqrt{f_\pm(x,t)}|1\rangle + \sqrt{1-f_\pm(x,t)}|0\rangle$.

(2) Collision step. Apply the collision operator simultaneously to all sites,

[1]Here we have taken the mass of a particle encoded in a qubit to be unity, $m=1$.

$$|\psi'(x,t)\rangle = \hat{U}|\psi(x,t)\rangle.$$

(3) Localization step. This step may be implemented in a nonunitary or unitary way. In the nonunitary way, the outgoing occupancy probability distribution is represented by the following matrix element:

$$f'_{\pm}(x,t) = \langle\psi'(x,t)|\hat{n}_{\pm}|\psi'(x,t)\rangle. \tag{18}$$

To recover the Burgers equation, $f_{\pm}$ can be determined by observation of a single system repeated enough times to recover the distribution (18) by equating to the frequency of occurrence of outcomes ("nonunitary read"). Alternatively, the phase of each qubit in the system can be periodically randomized by application of a unitary rotation of the qubits.

(4) Streaming step. Reinitialize ("write") the state of the quantum lattice gas as a separable state where each qubit is set as follows:

$$|q_{\pm}(x,t+\tau)\rangle = \sqrt{f'_{\pm}(x \mp \delta x,t)}|1\rangle + \sqrt{1-f'_{\pm}(x \mp \delta x,t)}|0\rangle \tag{19}$$

for all x. Note that qubit $|q_+\rangle$ is shifted to its neighboring node at the left while $|q_-\rangle$ is shifted to its neighboring node at the right. This step requires nearest-neighbor communication between all lattice nodes. At this point, one time-step update is completed.

III. ANALYTICAL TREATMENT

A. Quantum collision function

Here we shall derive (1) from (2). We begin with the outgoing occupation probabilities

$$f'_{\pm} = \langle\psi'|\hat{n}_{\pm}|\psi'\rangle = \langle\psi|\hat{U}^{\dagger}\hat{n}_{\pm}\hat{U}|\psi\rangle. \tag{20}$$

The initial on-site ket $|q_+\rangle \otimes |q_-\rangle$ is

$$|\psi\rangle = \sqrt{f_+f_-}|11\rangle + \sqrt{f_+(1-f_-)}|10\rangle + \sqrt{(1-f_+)f_-}|01\rangle + \sqrt{(1-f_+)(1-f_-)}|00\rangle \tag{21}$$

$$= \begin{pmatrix} \sqrt{(1-f_+)(1-f_-)} \\ \sqrt{(1-f_+)f_-} \\ \sqrt{f_+(1-f_-)} \\ \sqrt{f_+f_-} \end{pmatrix}. \tag{22}$$

We use a conservative quantum logic gate to represent the collision operator:

$$\hat{U} = \begin{pmatrix} 1 & 0 & 0 & 0 \\ 0 & e^{-i\xi}\cos\theta & -e^{-i\zeta}\sin\theta & 0 \\ 0 & e^{i\zeta}\sin\theta & e^{i\xi}\cos\theta & 0 \\ 0 & 0 & 0 & 1 \end{pmatrix}. \tag{23}$$

The qubit number operators are

$$\hat{n}_+ = \begin{pmatrix} 0 & 0 & 0 & 0 \\ 0 & 0 & 0 & 0 \\ 0 & 0 & 1 & 0 \\ 0 & 0 & 0 & 1 \end{pmatrix}, \quad \hat{n}_- = \begin{pmatrix} 0 & 0 & 0 & 0 \\ 0 & 1 & 0 & 0 \\ 0 & 0 & 0 & 0 \\ 0 & 0 & 0 & 1 \end{pmatrix} \tag{24}$$

Substituting Eqs. (22)–(24) into Eq. (20) gives us explicit update rules for the probability occupancies:

$$f'_+ = f_+f_- + \|e^{i\xi}\cos\theta\sqrt{f_+(1-f_-)} + e^{i\zeta}\sin\theta\sqrt{(1-f_+)f_-}\|^2 \tag{25a}$$

$$f'_- = f_+f_- + \|-e^{-i\zeta}\sin\theta\sqrt{f_+(1-f_-)} + e^{-i\xi}\cos\theta\sqrt{(1-f_+)f_-}\|^2, \tag{25b}$$

where the double vertical bars denote the norm or absolute value of the enclosed quantity. After some algebraic manipulation, this pair of equations can be reduced to the standard form

$$f_{\pm} \equiv \langle\psi'|\hat{n}_{\pm}|\psi'\rangle = f_{\pm} \pm \Omega(f_+,f_-). \tag{26}$$

On the RHS of (26), the quantum collision function $\Omega(f_+,f_-)$ is

$$\Omega(f_+,f_-) = -\sin^2\theta[f_+(1-f_-) - (1-f_+)f_-] + \sin 2\theta\cos(\zeta-\xi)\sqrt{f_+(1-f_+)f_-(1-f_-)}. \tag{27}$$

Other than the dependence of the Euler angles, there appears an unusual dependence on the square root of the occupation probabilities. This type of additional term is a consequence of the microscopic-scale quantum nature of the model which remains evident at the mesoscopic scale. This term gives rise to nonlinearity in the macroscopic equation of motion. The reason the square root term arises in (27) has its origin in the fundamental qubit encoding, described in Sec. II D, where the square root of the occupation probabilities is employed to generate the initial probability amplitudes of a qubit's two-level states. In turn, the local on-site ket appearing in (21) and (22) depends on the square root of the occupation probabilities. Inserting (22) into (20), and after working through some algebraic manipulations, we see that the mesoscopic collision operator too must depend explicitly on the value of a probability amplitude, and not just on classical probabilities. The fact that the square roots of probabilities are employed in the algorithm is a characteristic feature of its quantum-mechanical nature.

Equation (27) can be expressed a bit more simply:

$$\Omega(f_+,f_-) = \sin^2\theta(f_- - f_+) + \sin 2\theta\cos(\zeta-\xi)\sqrt{f_+(1-f_+)f_-(1-f_-)}. \tag{28}$$

B. Local equilibria

Let $d_{\pm}$ denote the local equilibrium values of the occupation probabilities. The equilibrium condition $\Omega(f_+,f_-)|_{f_{\pm}=d_{\pm}}=0$ becomes

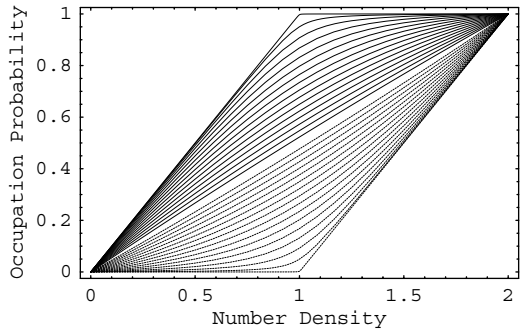

FIG. 2. A plot of the equilibrium occupancy probabilities $d_\pm$ versus the number density at that site. The upper solid curves are $d_+(\theta,\xi,\zeta)$ and the lower dotted curves are $d_-(\theta)$ as specified by Eq. (34) for $\theta=\pi/512,\ldots,\pi/2-\pi/512$ in steps of $\Delta\theta=\pi/32$ for $\xi=\zeta$. The abscissa and ordinate are both nondimensional probability values. $\theta=\pi/2$ is the diffusive case where $d_\pm=\rho/2$.

$$\frac{d_+}{1-d_+}-\frac{d_-}{1-d_-}=2\cot\theta\cos(\zeta-\xi)\sqrt{\frac{d_+}{1-d_+}\frac{d_-}{1-d_-}}, \tag{29}$$

which is a statement of detailed balance of collisions at the mesoscopic scale and which we analyze in Sec. IV B.

We take the equilibrium occupation probabilities to have the following form:

$$d_+=\frac{1}{\gamma z+1}\quad\text{and}\quad d_-=\frac{1}{z/\gamma+1}. \tag{30}$$

Substituting (30) into (29) gives a quadratic equation in γ that has the solution

$$\gamma=\sqrt{\alpha^2+1}+\alpha, \tag{31a}$$

$$\frac{1}{\gamma}=\sqrt{\alpha^2+1}-\alpha, \tag{31b}$$

where $\alpha\equiv\cot\theta\cos(\zeta-\xi)$. Next, substituting (30) into the total number density $\rho=d_++d_-$, we obtain a quadratic equation in z,

$$\rho z^2+\left(\gamma+\frac{1}{\gamma}\right)(\rho-1)z+\rho-2=0. \tag{32}$$

Substituting the positive root solution of (32) into (30), we find after much algebraic manipulation

$$d_+=\frac{1+\gamma^2+(1-\gamma^2)\rho-\gamma\sqrt{(1/\gamma+\gamma)^2(\rho-1)^2+4(\rho-2)\rho}}{2(1-\gamma^2)}. \tag{33}$$

Then substituting $\gamma=\sqrt{\alpha^2+1}+\alpha$ into (33) gives the result

$$d_\pm=\frac{\rho}{2}\mp\frac{1}{2\alpha}[\sqrt{1+\alpha^2}-\sqrt{1+\alpha^2(\rho-1)^2}]. \tag{34}$$

The local equilibria $d_\pm$ are plotted in Fig. 2 for a range of angles.

C. Chapman-Enskog expansion for the Burgers equation

It is convenient to treat the occupation probabilities as a two-component field

$$\mathbf{f}=\begin{pmatrix}f_+\\ f_-\end{pmatrix}. \tag{35}$$

We expand $\mathbf{f}$ about its equilibrium value denoted $\mathbf{d}$ so that $\mathbf{f}=\mathbf{d}+\delta\mathbf{f}+O(\varepsilon^2)$, where $\varepsilon\sim\delta x$ is analogous to what in the literature on fluid dynamics is called the *Knudsen number*.[2] The equilibrium condition $\Omega|_{\mathbf{f}=\mathbf{d}}=0$ leads to a tractable polynomial equation for the components of $\mathbf{d}$. The linearized finite-difference quantum Boltzmann equation is

$$\mathbf{f}(x\pm\delta x,t+\delta t)-\mathbf{f}(x,t)=J\delta\mathbf{f}(x,t), \tag{36}$$

where the Jacobian of the collision term is

$$\mathbf{J}\equiv\left.\begin{pmatrix}\partial\Omega/\partial a & \partial\Omega/\partial b\\ -\partial\Omega/\partial a & -\partial\Omega/\partial b\end{pmatrix}\right|_{\mathbf{f}=\mathbf{d}}=\begin{pmatrix}J_+ & J_-\\ -J_+ & -J_-\end{pmatrix}. \tag{37}$$

The left and right eigenvectors of J are

$$\xi^1=(1\quad 1),\quad \xi_1=\frac{1}{J_--J_+}\begin{pmatrix}J_-\\ -J_+\end{pmatrix}, \tag{38}$$

$$\xi^2=\frac{1}{J_+-J_-}(J_+\quad J_-),\quad \xi_2=\begin{pmatrix}1\\ -1\end{pmatrix}, \tag{39}$$

with associated eigenvalues $\lambda_1=0$ and $\lambda_2=J_+-J_-$. $\xi^i\xi_j=\delta_{ij}$. $\mathbf{J}$ may be rewritten as

$$\mathbf{J}=\lambda_2\xi_2\xi^2=\begin{pmatrix}J_+ & J_-\\ -J_+ & -J_-\end{pmatrix}. \tag{40}$$

$\mathbf{J}$ is singular. Its Moore-Penrose generalized inverse [47] is the following:

$$\mathbf{J}^{-1}_{\text{gen}}=\frac{1}{\lambda_2}\xi_2\xi^2=\frac{1}{J_+-J_-}\mathbf{J}. \tag{41}$$

Now we invoke the continuum limit where $\delta x\to 0$ and $\delta t\to 0$ so $\mathbf{f}$ is a continuous and differentiable two-component field. We obtain a first-order equation by Taylor-expanding (36) in x and t and keeping only terms first order in ε:

$$\sigma_z\delta x\partial_x\mathbf{d}=\mathbf{J}\delta\mathbf{f}+O(\varepsilon^2), \tag{42}$$

where $\sigma_z=\left(\begin{smallmatrix}1&0\\0&-1\end{smallmatrix}\right)$. Multiplying (42) on the left by $\mathbf{J}$ gives

$$\mathbf{J}\sigma_z\delta x\partial_x\mathbf{d}=(J_+-J_-)\mathbf{J}\delta\mathbf{f}+O(\varepsilon^2), \tag{43}$$

which has the nontrivial solution

$$\delta\mathbf{f}=\frac{1}{J_+-J_-}\sigma_z\delta x\partial_x\mathbf{d}+O(\varepsilon^2) \tag{44}$$

consistent with (41). Taking the difference of the respective components gives

[2] In this one-dimensional quantum model, the flow speed is proportional to the number density, $u=c_s(1-\rho)$. Therefore, requiring $\varepsilon\sim\delta\rho$ be small implies a low-Mach-number constraint. The analytical development is guaranteed to be valid only in the subsonic limit where $u\ll c_s$.

$$\delta f_+ - \delta f_- = \frac{1}{J_+ - J_-}\delta x \partial_x \rho + O(\varepsilon^2). \tag{45}$$

Similarly from (36), we obtain the second-order equation

$$\delta t \partial_t \mathbf{d} + \sigma_z \delta x \partial_x (\mathbf{d} + \delta \mathbf{f}) + \frac{\delta x^2}{2}\partial_{xx} d + O(\varepsilon^3) = \begin{pmatrix} \Omega \\ -\Omega \end{pmatrix}. \tag{46}$$

We now take the sum of the respective components:

$$\delta t \partial_t \rho + \delta x \partial_x (d_+ - d_- + \delta f_+ - \delta f_-) + \frac{\delta x^2}{2}\partial_{xx}\rho + O(\varepsilon^3) = 0. \tag{47}$$

Inserting (45) into the above equation gives the general effective field theory for any one-dimensional two-qubit-per-site lattice gas conserving particle number,

$$\partial_t \rho + c\partial_x (d_+ - d_-) + \frac{\delta x^2}{\delta t}\frac{\partial_x (J_+ - J_-)}{(J_+ - J_-)^2}\partial_x \rho + \frac{\delta x^2}{2\delta t}\left(\frac{2}{J_+ - J_-} + 1\right)\partial_{xx}\rho + O(\varepsilon^3) = 0. \tag{48}$$

Equation (34) implies that

$$d_+ - d_- = -\frac{1}{\alpha}[\sqrt{1+\alpha^2} - \sqrt{1+\alpha^2(\rho - 1)^2}]. \tag{49}$$

Again, we compute the components of J:

$$J_\pm = \frac{\partial \Omega}{\partial p_\pm} = \sin^2\theta\left(\mp 1 - \alpha\frac{(2d_\pm - 1)d_\mp(1-d_\mp)}{\sqrt{d_+(1-d_+)d_-(1-d_-)}}\right). \tag{50}$$

And this implies

$$J_+ - J_- = -2\sin^2\theta(1 + \alpha^2 \mathcal{R}), \tag{51}$$

where the factor $\mathcal{R} = \mathcal{R}(\alpha, \rho)$ is too complicated an expression to write out here but has the important property that $\mathcal{R}(\alpha, \rho) = 1 + O(\alpha)$. Finally, substituting the two results (49) and (51) into (48) gives the effective field theory

$$\partial_t \rho + c\cot\theta\cos(\zeta - \xi)(1-\rho)\partial_x \rho = \frac{\cot^2\theta}{2}\frac{\delta x^2}{\delta t}\partial_{xx}\rho + O(\varepsilon^3, \varepsilon\alpha^2), \tag{52}$$

which becomes identical to (1) for $u = c_s(1-\rho)$ with sound speed $c_s = c\cot\theta\cos(\zeta - \xi)$ and kinematic viscosity $\nu = \frac{1}{2}\cot^2\theta\,\delta x^2/\delta t$. c_s and ν are "programmable" by appropriately choosing the Euler angles in (23).

IV. STABILITY CONSIDERATIONS

A. Quantum-mechanical entropy function

The unconditional numerical stability of the quantum algorithm can be understood from another vantage point which clarifies the statement of the unitarity of the quantum-mechanical collision process. There exists an entropy function, denoted here as $\mathcal{H}$, that is consistent with the unitary collision operator (23), the Fermi-Dirac equilibrium for the occupation probabilities of the qubit's eigenstates (30), the quantum Boltzmann equation (20), and the nonlinear quantum collision function (28). The quantum-mechanical entropy function is

$$\mathcal{H} = -\sum_{a=\pm}[f_a \ln(\gamma_a f_a) + (1 - f_a)\ln(1 - f_a)], \tag{53}$$

where $\gamma_+ = \sqrt{\alpha^2+1} + \alpha$, $\gamma_- = 1/\gamma_+ = \sqrt{\alpha^2+1} - \alpha$. Let $E_\pm$ denote the qubit energy eigenvalues. If we calculate the maximum of the entropy function, $\partial\mathcal{H}/\partial f_a = 0$, where we add the Lagranian multiplier $\beta E_\pm f_\pm$ to $\mathcal{H}$ as a conserved energy constraint, we find that the solution for $f_\pm$ is (30). That is,

$$\frac{\partial \mathcal{H}}{\partial f_\pm} = -\ln(\gamma_\pm f_\pm) - 1 + \ln(1 - f_\pm) + 1 + \beta E_\pm, \tag{54}$$

from which we can solve for the nonequilibrium distribution function,

$$f_\pm^{\text{noneq}} = \frac{1}{(1/\gamma_\pm)e^{\beta E_\pm - \partial_{f_\pm}\mathcal{H}} + 1}. \tag{55}$$

The equilibrium point occurs at $\partial_{f_\pm}\mathcal{H} = 0$, so from (55) we obtain the Fermi-Dirac function

$$f_\pm^{\text{eq}} = \frac{1}{(1/\gamma_\pm)e^{\beta E_\pm} + 1}. \tag{56}$$

We can also check whether (53) is consistent with the quantum collision function (28). To do this, we express (28) in terms of the macroscopic variables $\rho = f_+ + f_-$ and $v \equiv f_+ - f_-$ as follows:

$$\Omega_{\text{qu}}(\rho, v) = -\sin^2\theta\, v + \frac{1}{2}\sin 2\theta\cos\xi\sqrt{(\rho^2 - v^2)\left(1 - \rho + \frac{1}{4}(\rho^2 - v^2)\right)}. \tag{57}$$

The equilibrium contours of constant v, the kinetic mode defined by (49), are shown on the top of Fig. 3. Since ρ is conserved, the quantum Boltzmann equation (20) reexpressed in terms of the macroscopic variables acts only on the kinetic mode:

$$v' = v + 2\Omega_{\text{qu}}(\rho, v). \tag{58}$$

We can also express the entropy function in terms of the macroscopic variables:

$$\mathcal{H}_\gamma(\rho, v) = 2\ln 2 - \frac{1}{2}\left((\rho + v)\ln[\gamma(\rho + v)] + (\rho - v)\ln\frac{\rho - v}{\gamma} + (2 - \rho + v)\ln(2 - \rho + v) + (2 - \rho - v)\ln(2 - \rho - v)\right). \tag{59}$$

The entropy function $\mathcal{H} = \mathcal{H}_\gamma(\rho, v)$ is indirectly a function of the Euler angles of the quantum logic gate since $\gamma = \gamma(\theta, \xi, \zeta)$. Constant-entropy contours of the surface defined by (59) are shown at the right of Fig. 3.

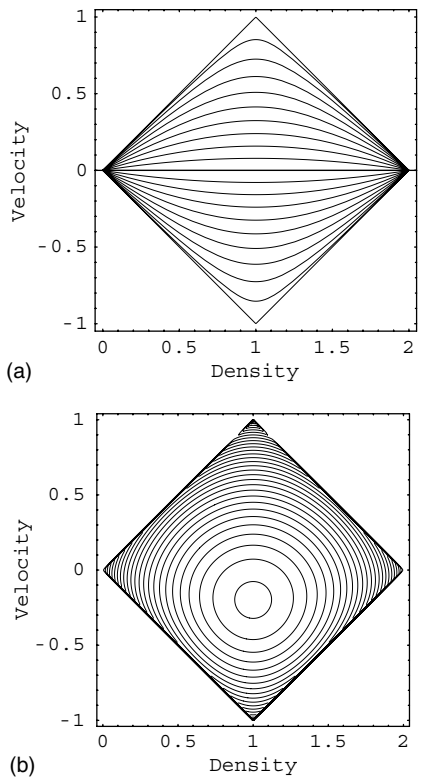

FIG. 3. (a) equilibria contours of the kinetic mode $v^{\mathrm{eq}}=d_+-d_-$. (b) constant-entropy contours of $\mathcal{H}_\gamma(\rho,v)$ for $\theta=1.5$ rad.

B. Detailed balance

1. Transition matrix and detailed balance

With two qubits located per lattice node, there are four basis states:

$$s_0=|00\rangle,\quad f_+=0\quad f_-=0,\quad P_0=(1-d_+)(1-d_-),$$

$$s_1=|01\rangle,\quad f_+=0,\quad f_-=1,\quad P_1=(1-d_+)d_-,$$

$$s_2=|10\rangle,\quad f_+=1,\quad f_-=0,\quad P_2=d_+(1-d_-),$$

$$s_3=|11\rangle,\quad f_+=1,\quad f_-=1,\quad P_3=d_+d_-. \tag{60}$$

In (60), the configuration probabilities P_i, for $i=0,1,2,3$, are mean-field estimates neglecting qubit-qubit correlations. Using Q qubits to encode up to Q fermions, there are 2^Q quantum states. We shall consider the $Q=2$ case:

$$\begin{pmatrix} P_0' \\ P_1' \\ P_2' \\ P_3' \end{pmatrix} = \underbrace{\begin{pmatrix} T_{00} & T_{01} & T_{02} & T_{03} \\ T_{10} & T_{11} & T_{12} & T_{13} \\ T_{20} & T_{21} & T_{22} & T_{23} \\ T_{30} & T_{31} & T_{32} & T_{33} \end{pmatrix}}_{\text{transition matrix}} \begin{pmatrix} P_0 \\ P_1 \\ P_2 \\ P_3 \end{pmatrix}. \tag{61}$$

Conservation of probability condition is

$$\sum_{i=0}^{2^Q-1} P_i' = \sum_{i=0}^{2^Q-1} P_i, \tag{62}$$

which implies

$$\sum_{i=0}^{2^Q-1}\left(\sum_{j=0}^{2^Q-1} T_{ij}P_j - P_i\right) = \sum_{j=0}^{2^Q-1} P_j\left(\sum_{i=0}^{2^n-1} T_{ij}\right) - \sum_{j=0}^{2^Q-1} P_j = 0, \tag{63}$$

provided the columns of the transition matrix sum to unity. Hence, to conserve probability, we require

$$\sum_{i=0}^{2^Q-1} T_{ij} = 1. \tag{64}$$

2. Conservative transition matrix

The detailed balance condition is stated as follows:

$$T_{ij}P_i = T_{ji}P_j, \tag{65}$$

for $i\neq j$. To conserve particle number, the transition matrix for the $Q=2$ case is constrained to have the form

$$\mathbf{T}_{\text{conservative}} = \begin{pmatrix} 1 & 0 & 0 & 0 \\ 0 & 1-A-C & A+D & 0 \\ 0 & B+C & 1-B-D & 0 \\ 0 & 0 & 0 & 1 \end{pmatrix}, \tag{66}$$

where the rows sum to unity according to (64) to preserve probability $(P_1'+P_2'=P_1+P_2)$, so we have

$$P_1'+P_2' = (1-A-C)P_1 + (A+D)P_2 + (B+C)P_1 + (1-B-D)P_2. \tag{67}$$

This implies

$$P_1+P_2 = (1-A+B)P_1 + (1+A-B)P_2 \tag{68}$$

or

$$(B-A)(P_1-P_2) = 0. \tag{69}$$

The detailed balance condition (65) for $i=1$ and $j=2$ is

$$(A+D)P_1 = (B+C)P_2. \tag{70}$$

The set of equations (69) and (70) admits two solutions. The first solution (diffusion case) is the following: $A=B$ and $C=D$ with identical local equilibria $P_1=P_2$. In the mean-field limit, we can write $P_1=(1-d_+)d_-$ and $P_2=d_+(1-d_-)$, so the equality $P_1=P_2$ implies that the equilibrium occupation probabilities are equal as well, $d_+=d_-$. This solution can be parametrized by an angle θ where in (66) $A=B=\sin^2\theta$:

$$\mathbf{T}_{\text{doubly stochastic}} = \begin{pmatrix} 1 & 0 & 0 & 0 \\ 0 & \cos^2\theta - C & \sin^2\theta + C & 0 \\ 0 & \sin^2\theta + C & \cos^2\theta - C & 0 \\ 0 & 0 & 0 & 1 \end{pmatrix}. \tag{71}$$

Equation (71) leads to the constraint $(P_2/P_1-1)(\sin^2\theta+C)=0$, which in turn gives $P_1=P_2$.

The second solution (Burgers case) of (69) and (70) is the following: $A=B$ and $C\neq D$ with nonequal local equilibria $P_1\neq P_2$. In this case, the transition matrix is not doubly stochastic. There is no transition matrix that is doubly stochastic that gives rise to a situation where $P_1\neq P_2$. We will see in Sec. IV B 3 that the transition matrix of the quantum model has this second form:

$$\mathbf{T}_{\text{qm}} = \begin{pmatrix} 1 & 0 & 0 & 0 \\ 0 & \cos^2\theta - C & \sin^2\theta + D & 0 \\ 0 & \sin^2\theta + C & \cos^2\theta - D & 0 \\ 0 & 0 & 0 & 1 \end{pmatrix}, \tag{72}$$

where the particular values of $C=C(\theta,\xi,\zeta,\psi_1,\psi_2)$ and $D=D(\theta,\xi,\zeta,\psi_1,\psi_2)$ will be determined by the Euler angles in the unitary collision operator (23) and the probability amplitudes of the quantum state vector.

At equilibrium, using (30), $P_1/P_2=\gamma^2$, so the detailed balance condition (70) in this case is

$$\gamma^2 = \frac{\sin^2\theta + C}{\sin^2\theta + D}. \tag{73}$$

A solution is the following:

$$C = \frac{\gamma \sin 2\theta}{2} e^{i(\xi-\zeta)}, \tag{74a}$$

$$D = -\frac{\sin 2\theta}{2\gamma} e^{-i(\xi-\zeta)}. \tag{74b}$$

Since C and D depend on γ, this means the components of the transition matrix will in turn depend on the state probabilities because $\gamma=\sqrt{P_1/P_2}$. The dynamics remains intrinsically nonlinear. Inserting (74) into (73) gives the following quadratic equation for γ:

$$\sin^2\theta\gamma^2 - \sin 2\theta\cos(\xi-\zeta)\gamma - \sin^2\theta = 0. \tag{75}$$

This has a solution

$$\gamma = \sqrt{\cot^2\theta\cos^2(\xi-\zeta)+1} + \cot\theta\cos(\xi-\zeta), \tag{76}$$

which is exactly (31). Hence, (74) is a consistent solution since $\gamma=\gamma(\theta,\xi,\zeta)$.

3. Quantum transitions

Here we derive the mesoscopic stochastic transition matrix (72) along with the parameters (74) by starting directly from the quantum unitary evolution. To do this, we begin by writing the quantum-mechanical collision transformation acting on the microscopic quantum state as a general block-diagonal unitary matrix with complex coefficients:

$$\begin{pmatrix} \psi_0' \\ \psi_1' \\ \psi_2' \\ \psi_3' \end{pmatrix} = \begin{pmatrix} 1 & 0 & 0 & 0 \\ 0 & U_{11} & U_{12} & 0 \\ 0 & U_{21} & U_{22} & 0 \\ 0 & 0 & 0 & U_{33} \end{pmatrix} \begin{pmatrix} \psi_0 \\ \psi_1 \\ \psi_2 \\ \psi_3 \end{pmatrix} \tag{77}$$

The unitarity condition $(\hat{U}^\dagger\hat{U}=\mathbb{I})$ constrains the complex coefficients as follows:

$$|U_{11}|^2 + |U_{21}|^2 = 1, \quad U_{11}^* U_{12} + U_{21}^* U_{22} = 0,$$

$$U_{12}^* U_{11} + U_{22}^* U_{21} = 0, |U_{12}|^2 + |U_{22}|^2 = 1,$$

$$U_{33}^* U_{33} = 1. \tag{78}$$

The quantum-state incoming probabilities are defined as follows:

$$P_0 \equiv |\psi_0|^2, \quad P_1 \equiv |\psi_1|^2, \quad P_2 \equiv |\psi_2|^2, \quad P_3 \equiv |\psi_3|^2, \tag{79}$$

and, likewise, the quantum-state outgoing probabilities are

$$P_0' \equiv |\psi_0'|^2, \quad P_1' \equiv |\psi_1'|^2, \quad P_2' \equiv |\psi_2'|^2, \quad P_3' \equiv |\psi_3'|^2. \tag{80}$$

From Eq. (77) we see that

$$|\psi_0'|^2 = |\psi_0|^2, \tag{81a}$$

$$|\psi_1'|^2 = (U_{11}^*\psi_1^* + U_{12}^*\psi_2^*)(U_{11}\psi_1 + U_{12}\psi_2), \tag{81b}$$

$$|\psi_2'|^2 = (U_{21}^*\psi_1^* + U_{22}^*\psi_2^*)(U_{21}\psi_1 + U_{22}\psi_2), \tag{81c}$$

$$|\psi_3'|^2 = |\psi_3|^2, \tag{81d}$$

which can be rewritten as a quantum transition map,

$$P_0' = P_0, \tag{82a}$$

$$P_1' = |U_{11}|^2 P_1 + |U_{12}|^2 P_2 + U_{11}^* U_{12}\psi_1^*\psi_2 + U_{12}^* U_{11}\psi_1\psi_2^*, \tag{82b}$$

$$P_2' = |U_{21}|^2 P_1 + |U_{22}|^2 P_2 + U_{21}^* U_{22}\psi_1^*\psi_2 + U_{22}^* U_{21}\psi_1\psi_2^*, \tag{82c}$$

$$P_3' = P_3. \tag{82d}$$

In matrix form this becomes

$$\begin{pmatrix} P_0' \\ P_1' \\ P_2' \\ P_3' \end{pmatrix} = \underbrace{\begin{pmatrix} 1 & 0 & 0 & 0 \\ 0 & |U_{11}|^2 & |U_{12}|^2 & 0 \\ 0 & |U_{21}|^2 & |U_{22}|^2 & 0 \\ 0 & 0 & 0 & 1 \end{pmatrix}}_{\text{classical diffusive part}} \begin{pmatrix} P_0 \\ P_1 \\ P_2 \\ P_3 \end{pmatrix} + \underbrace{\begin{pmatrix} 0 \\ U_{11}^* U_{12} \psi_1^* \psi_2 + U_{12}^* U_{11} \psi_1 \psi_2^* \\ U_{21}^* U_{22} \psi_1^* \psi_2 + U_{22}^* U_{21} \psi_1 \psi_2^* \\ 0 \end{pmatrix}}_{\text{quantum-mechanical part}}. \tag{83}$$

The classical part of (83) is exactly (71). The quantum-mechanical part gives rise to nondiffusive advective behavior, which leads to nonlinear shock formation characteristic of the Burgers equation. Finally, from (83) we have a quantum transition matrix:

$$\mathbf{T}_{\text{qm}} = \begin{pmatrix} 1 & 0 & 0 & 0 \\ 0 & |U_{11}|^2 + U_{11}^* U_{12} \psi_2/\psi_1 & |U_{12}|^2 + U_{12}^* U_{11} \psi_1/\psi_2 & 0 \\ 0 & |U_{21}|^2 + U_{21}^* U_{22} \psi_2/\psi_1 & |U_{22}|^2 + U_{22}^* U_{21} \psi_1/\psi_2 & 0 \\ 0 & 0 & 0 & 1 \end{pmatrix}. \tag{84}$$

Equation (84) conserves probability ($\Sigma_i^3 P_i' = \Sigma_i^3 P_i$) due to unitarity, so its columns sum to unity owing to the unitary condition (78).

Now with the equilibrium probability amplitudes

$$\psi_0 = \sqrt{(1-d_+)(1-d_-)}, \tag{85a}$$

$$\psi_1 = \sqrt{(1-d_+)d_-}, \tag{85b}$$

$$\psi_2 = \sqrt{(d_+(1-d_-)}\,, \tag{85c}$$

$$\psi_3 = \sqrt{d_+ d_-}, \tag{85d}$$

and using (30), we see that

$$\frac{\psi_1}{\psi_2} = \sqrt{\left(\frac{d_-}{1-d_-}\right)\left(\frac{1-d_+}{d_+}\right)} = \gamma,$$

so that (84) becomes

$$\mathbf{T}_{\text{qm}}^{\text{eq}} = \begin{pmatrix} 1 & 0 & 0 & 0 \\ 0 & \cos^2\theta - \dfrac{e^{i(\xi-\zeta)}\sin 2\theta}{2\gamma} & \sin^2\theta - \dfrac{\gamma e^{-i(\xi-\zeta)}\sin 2\theta}{2} & 0 \\ 0 & \sin^2\theta + \dfrac{e^{i(\xi-\zeta)}\sin 2\theta}{2\gamma} & \cos^2\theta + \dfrac{\gamma e^{-i(\xi-\zeta)}\sin 2\theta}{2} & 0 \\ 0 & 0 & 0 & 1 \end{pmatrix}, \tag{86}$$

where γ is determined by (31). The equilibrium value of the quantum transition matrix (86) is identical to (72) with components (74).

V. SIMULATION RESULTS

A. Consistency of the entropy and collision functions

Figure 4 is a composite plot showing the $\mathcal{H}_\gamma$ function constant-density contours graphed for $\rho=0.7$ and $\xi=\zeta=0$, but each curve has a different Euler angle θ. The top curve is for $\theta=0.5708$ rad, correspondings to a high-viscosity model with $\nu=2.425\,48\delta x^2/\delta t$. The intermediate $\mathcal{H}_\gamma$ curves are plotted with θ incremented by $\Delta\theta=0.5$ rad. The bottom curve has $\theta=1.5708\ \text{rad}\simeq\pi/2$, which is a nearly inviscid contour of the entropy surface corresponding to an extremely low viscosity of $\nu=(1.34\times10^{-11})\delta x^2/\delta t$. The abscissa is the

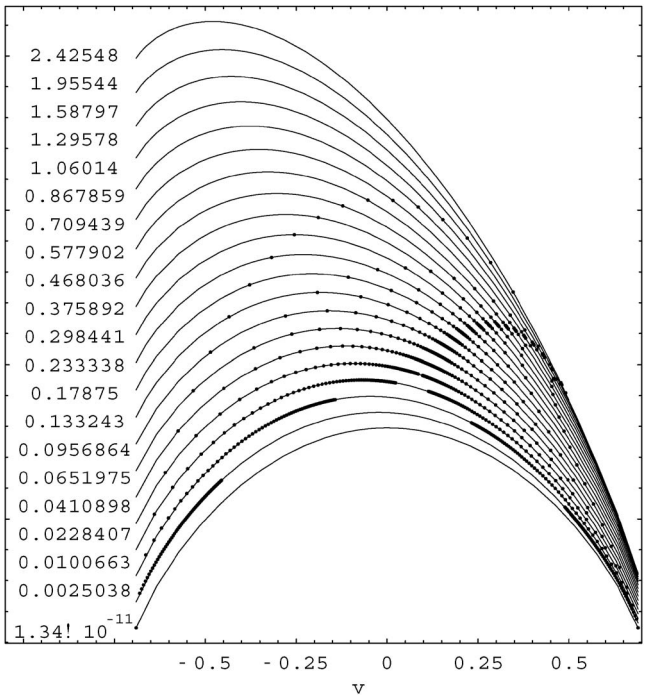

FIG. 4. $\mathcal{H}_\gamma$ function constant-density contours of the entropy surface (solid gray curves), which are vertically stacked over one another for graphical clarity. The x axis is $v=f_+-f_-$ and the y axis is entropy as defined by (59). The dynamical trajectories (black dots) were computed using the nonlinear quantum collision function $\Omega_{\rm qu}(\rho,v)$ for different values of the shear viscosity for a relatively high value of $\nu=2.425\,48\delta x^2/\delta t$ (on the top) down to an extremely low value of $\nu=(1.34\times10^{-11})\delta x^2/\delta t$ (at the bottom). Viscosity values are labeled on the left of the corresponding $\mathcal{H}_\gamma$ contours, not numerical values of the entropy.

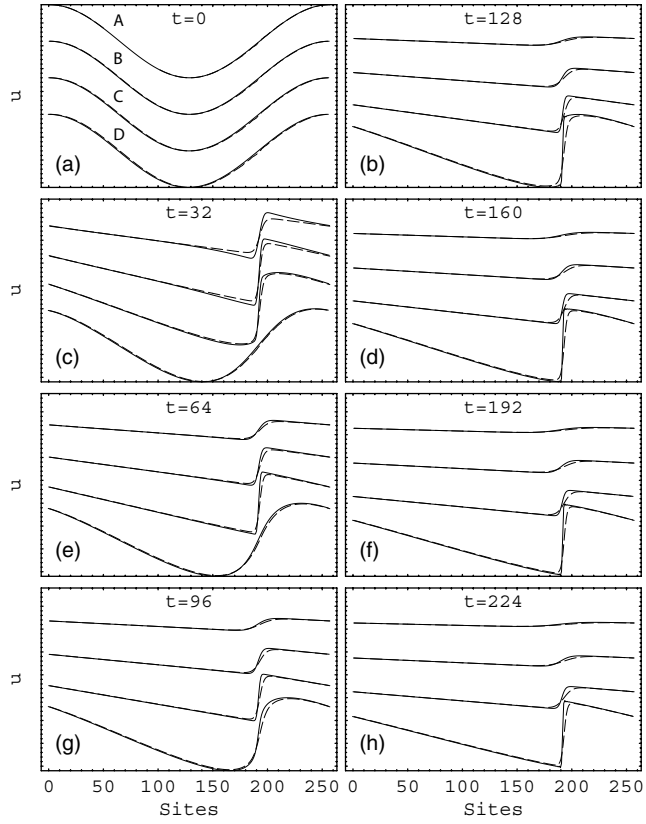

FIG. 5. Development of a shock front in the flow field $u(x,t)$ after the system is initialized with a sinusoidal profile on an $L=256$ site lattice for four different viscosities: (A) $\nu=8$, (B) 2, (C) 1/2, (D) 1/32, where the viscosity is in lattice units $\delta x^2/\delta t$. The curves are shifted vertically one from the other by $\Delta\rho=1/2$ to avoid overlapping. Agreement between the numerical data (solid curves) and the analytical solution (dashed curves) is excellent. The shock fronts of the analytical solutions are slightly wider than the shock fronts of the numerical simulations which have much sharper edges. This is because these plotted analytical solutions are slightly overdamped to help stabilize the series solution (89), so the quantum model data are more accurate approximations of the time-dependent solution to the Burgers equation. All four cases were initialized using (87) with $\rho_a=1$ and $\rho_b=0.4$.

kinetic mode $v=f_+-f_-$ plotted over the range $-\rho\geqslant v\geqslant\rho$ for $\rho=0.7$. The ordinate is the $\mathcal{H}_\gamma$ function plotted over the range $-0.5\geqslant\mathcal{H}_\gamma\geqslant2.0$. Each set of dynamical trajectory points computed using (58) exactly lie on the respective $\mathcal{H}_\gamma$ function contour, demonstrating the consistency of the quantum Boltzmann equation and the entropy function descriptions.

In the inviscid limit where $\theta\to\pi/2$, the quantum collision function reduces to $\Omega_{\rm qu}(\rho,v)=-v$, and in turn (58) reduces to $v'=-v$. So, as the fluid's viscosity is reduced, the collision process causes the sign of the velocity field to alternate. This is shown in Fig. 4, where for the lower-viscosity cases, the value of the kinetic mode jumps from the left $(-v)$ to the right side $(+v)$ of the entropy contour and back again.

B. Comparison to the Cole-Hopf solution

Choosing three sets of "Euler" angles in (23) to be $\theta=\pi/12.8239$ (case A), $\pi/6.77582$ (case B), $\pi/4$ (case C) and $\theta=\pi/2.36955$ (case D), and $\xi=\zeta$, then $\nu=8\delta x^2/\delta t$ (case A), $2\delta x^2/\delta t$ (case B), $\delta x^2/2\delta t$ (case C), and $\delta x^2/32\delta t$ (case D) are the corresponding shear viscosity transport coefficients. For these four cases, we compare the numerical prediction that the macroscopic scale behavior of the quantum algorithm is governed by the Burgers equation (1) with the exact solutions obtained by analytical means. For the purposes of the numerical tests, the system is simulated directly at the mesoscopic scale using (26), and all initialized with the same sinusoidal profile in the number density field

$$\rho(x_l,0)=\rho_a\cos\left(\frac{2\pi l}{L}\right)+\rho_b, \tag{87}$$

where $\rho_a=0.4$ and $\rho_b=1$, and $L=256$. A time history of the dynamical evolution of the number density fields is plotted in Fig. 5. The analytical solution of the Burgers equation is obtained by application of the Cole-Hopf transformation[3]

[3]It is possible to add an external noise term into the right-hand side of the Burgers equation (1) of the form $\partial\eta(x,t)/\partial x$. The potential field $h(x,t)$ is defined as follows: $\partial h(x,t)/\partial x\equiv u(x,t)$. Then $h(x,t)$ satisfies the Kardar-Parisi-Zhang equation [59].

$$\rho = \rho_a + \frac{2\nu}{c\psi}\frac{\partial \psi}{\partial x}, \tag{88}$$

where

$$\psi \equiv I_0(z) + 2\sum_{\ell=1}^{\infty} (-1)^{\text{floor}[\ell/2]} I_\ell(z) F_\ell(2\pi\ell x + \nu_\ell t) e^{-\mu_\ell t}, \tag{89}$$

and where $z \equiv c_s \rho_b / 4\pi\nu$, $\mu_\ell \equiv \nu(2\pi\ell)^2$, $\nu_\ell \equiv c_s(1-\rho_a)(2\pi\ell)$, the I_ℓ's are modified Bessel functions, and the function F_ℓ denotes the sine or cosine function when ℓ is odd or even, respectively,

$$F_\ell(x) \equiv \frac{(-1)^\ell + 1}{2}\cos(x) - \frac{(-1)^\ell - 1}{2}\sin(x). \tag{90}$$

To match the numerical simulations, the parameters in the analytical solution (89) were set to $c = Lc_s = 256 \cot\theta\, \delta x/\delta t$ and $\nu = \frac{1}{2}\cot^2\theta\, \delta x^2/\delta t$. Also in (89) the size of the system is set to unit length, $0 \leqslant x \leqslant 1$.

The agreement between the numerical prediction and the analytical solution is excellent for all cases, as shown in Fig. 5. There is a slight discrepancy between the analytical and numerical results after the shock front has developed in the flow field. The discrepancy occurs at the corners or edges of the shock. The analytical solution appears to be smoother across the shock front than the numerical solution. To plot the analytical solution, it was not possible to include all terms in the series expansion (89) from $\ell = 1$ up to $\ell = \infty$. Instead, an approximation was made using only the first 80 terms in the expansion (89). For cases when the shock front is too steep, the analytical solution diverges at shock front while the quantum algorithm remains unconditionally stable; it becomes computationally difficult to compute the analytically predicted exact solution using (89). To avoid this situation, some additional damping was added to the analytical series solution to ensure its convergence. This explains the observed discrepancy.

C. Near-inviscid flow

Figure 6 shows the time evolution of the same quantum lattice-gas system with $L = 256$ nodes. There are two situations with the collision operators set with different values for the Euler angles: $\nu = \delta x^2/2\delta t$ (dotted curve) and $\nu = 0.002\,514\,46\,\delta x^2/\delta t$ (solid curve) cases. The vertical axis is ρ plotted in the range of $\frac{1}{2} \leqslant \rho \leqslant \frac{3}{2}$. The time step is in the upper left corner of each snapshot. The viscosity of the quantum model is close to zero. The quantum algorithm is unconditionally stable and obeys the principle of detailed balance. Having a variable transport coefficient that can be made small, it is consistent with the inviscid Burgers equations when the Euler angle $\theta \simeq \pi/2$. The numerical simulation result plotted in Fig. 7 manifests a characteristic property of a type-II quantum algorithm. The expected values of the occupancy of the ground and excited states of a microscopic qubit contained within a quantum-mechanical node of the lattice are shifted. The expectation value of the excited state is plotted in the blue curve shown in Fig. 7(b). Regardless of the

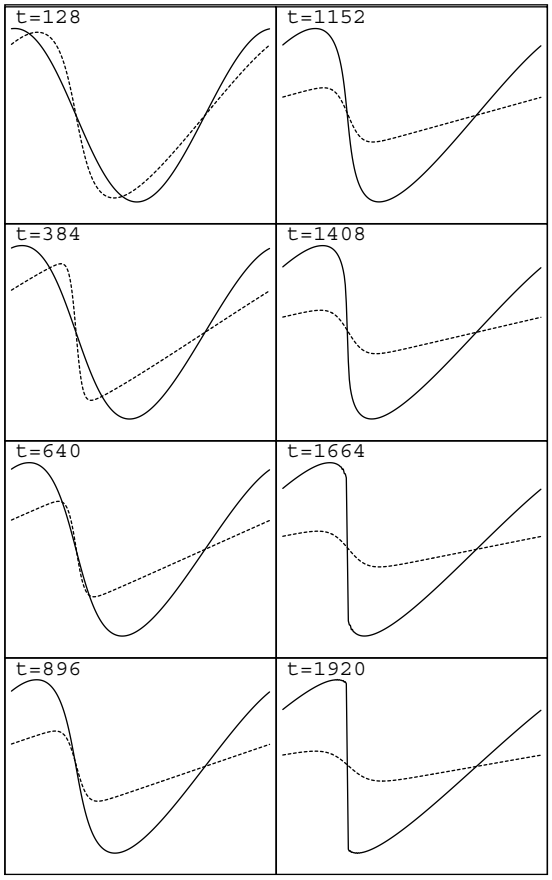

FIG. 6. Two scenarios: the quantum lattice gas with $\theta = 1.5$ rad and $\zeta = \xi = 0$ (solid curve) and $\theta = \pi/4$ and $\zeta = \xi = 0$ (dotted curve). This demonstrates a quantum lattice gas modeling a low-viscosity fluid when $\theta \simeq \pi/2$.

dissipation regime (high or low viscosity), there is a gap in the values of the occupation probabilities; hence, $d_+ \neq d_-$. The physical cause of this gap is the following. The microscopic dynamics is interpreted as the motion of qubits moving left and right through a chain of quantum processors. If the likelihood of a qubit exiting left or right from a quantum processor is equal, then the excited-state energies encoding the left- and right-going probabilities will be degenerate. The equilibrium probabilities must overlap: $d_+ = d_-$. The macroscopic effective field theory would be strictly diffusive as any qubit would move up and down the one-dimensional chain of quantum processors in an unbiased random walk fashion. However, if the likelihood of a qubit exiting a quantum processor to the left does not equal the likelihood it will exit to the right, then the degeneracy in the distribution functions is lifted and an energy gap appears as demonstrated in Fig. 7. In this case, the macroscopic effective field theory would not be strictly diffusive; there would be an overall net advection of qubits in one direction (the symmetry of the lattice is broken and this causes an energy gap in excited-state energy levels). This net advection gives rise to the nonlinear terms in (1).

In regions of $\partial v/\partial x < 0$, shocks tend to form in the v field. Asymptotically, v attains a constant slope with shock

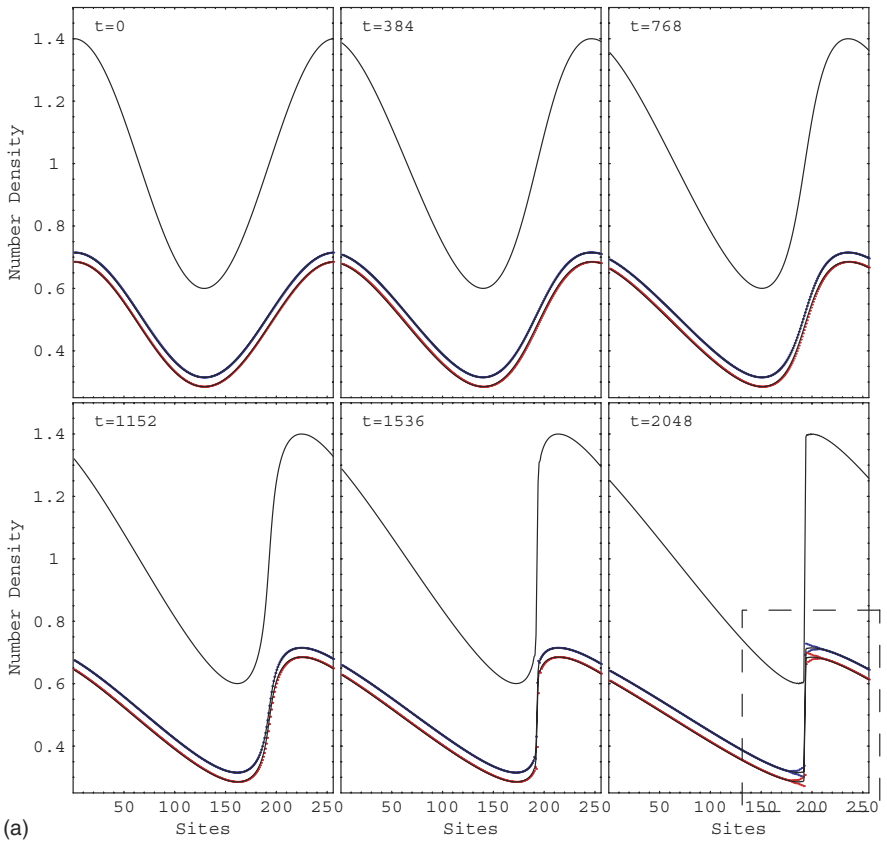

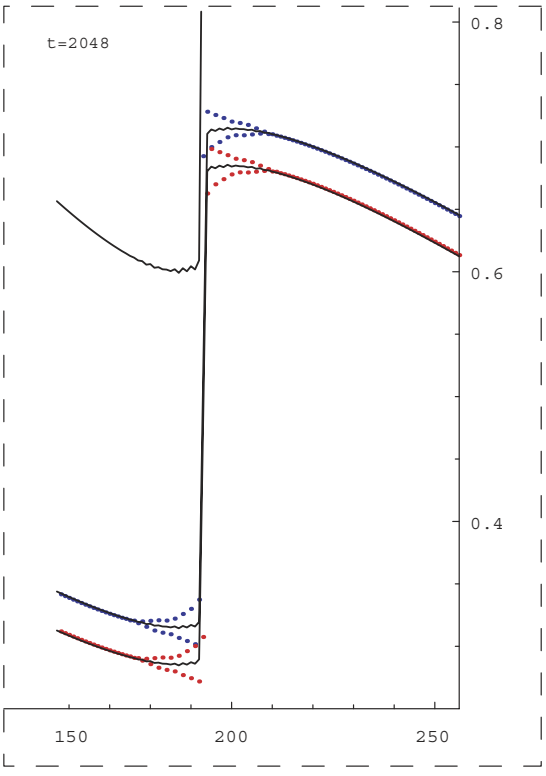

FIG. 7. (Color online) Highly underresolved simulation with $\theta = 1.5$ rad with $L = 256\delta x$. (a) Six successive snapshots of the flow field data (black curve) and the numerical prediction of the occupancy probabilities f_+ (blue dots) and f_- (red dots). The analytically predicted equilibria, d_+ and d_-, are overplotted (black curves). There is excellent agreement between theory and simulation, with a deviation occurring at late times after the shock front is fully formed. (b) An expanded view of the shock front at $t = 2048\delta x/\delta t$. The width of the shock front is much less than δx so a kind of Gibbs oscillation emerges.

discontinuities. In Fig. 7, the extent of the Gibbs oscillations at the shock front is greater at the mesoscopic than at the macroscopic scale because of a fortuitous cancellation of errors. In Fig. 8, we compare the analytically predicted values of the equilibrium distribution to the numerically obtained distribution. There is excellent agreement in the high-dissipation regime, shown in the top graph in Fig. 8. However, a discrepancy emerges in the extremely low-dissipation regime, shown in the bottom graph in Fig. 8, which corresponds to the underresolved shock front.

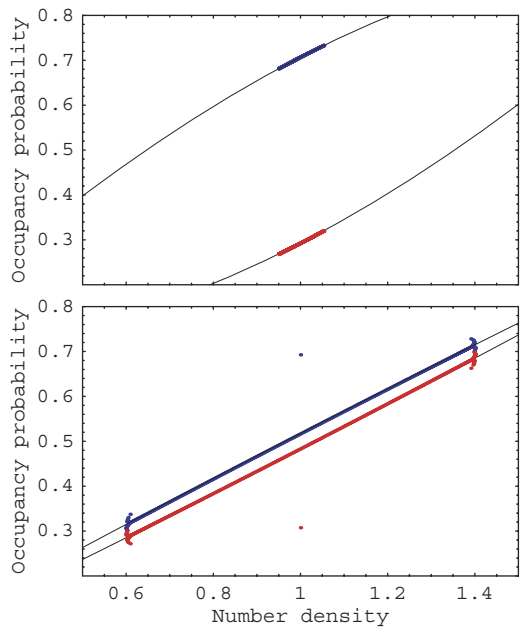

FIG. 8. (Color online) Analytical versus numerical equilibria: (top plot) high viscosity $\theta=\pi/4$ rad, and (bottom plot) low viscosity $\theta=1.5$ rad. The numerical data of the occupancy probabilities f_+ (blue dots) and f_- (red dots) are shown for the flow field at $t=2048\delta t$. The analytically predicted equilibria, d_+ and d_-, plotted as well (black curves). In the low-viscosity case, the deviation of the occupancy probabilities for the highest and lowest values of the number density corresponds to the aberrant Gibbs oscillations seen in Fig. 7 of the under-resolved flow.

VI. FINAL REMARKS

An open system quantum model for the nonlinear Burgers equations was presented. A salient feature of this microscopic quantum model is that at the mesoscopic scale the model effectively behaves as a kinetic system of qubits accurately governed by a quantum Boltzmann equation of motion. As a consequence of the microscopic unitarity of the quantum-mechanical evolution operator, the mesoscopic-scale qubit dynamics obeys statistical detailed balance in its collisions. Furthermore, the dynamics obeys an entropy theorem consistent with the second law of thermodynamics. A feature of the model is that it allows for arbitrary tuning of the macroscopic-scale shear viscosity transport coefficient. Localization of the microscopic dynamics, for example through state reduction via a measurement process, allows for tuning the level of the consequent macroscopic scale dissipation. This feature is important from a computational physics perspective because the model, seen as a quantum algorithm, remains unconditionally stable at extremely low dissipation regimes. This allows us to use the quantum algorithm for modeling highly nonlinear shock formation, even severely under-resolved shock fronts, without the model breaking down. All numerical tests of the algorithm indicate that the analytical treatment of the quantum model is correct.

The quantum lattice Boltzmann equation that represents our quantum algorithm can be directly implemented on a present-day classical computer (so long as the number of qubits per quantum node is small) and constitutes a new modeling tool for numerically predicting the time-dependent behavior of hydrodynamic flow and shock formation. This quantum Boltzmann equation method, which is akin to the entropic lattice Boltzmann equation method [48–55], and which in turn was an offshoot of the lattice Boltzmann equation method [56], when implemented on a present-day supercomputer can be generalized to model Navier-Stokes turbulence. A subsequent paper on this subject will present recent simulation results for turbulent fluid dynamics using the quantum Boltzmann equation method.

The quantum Boltzmann equation method in this paper has also been extended to handle magnetohydrodynamics in one spatial dimension where the shear viscosity and resistivity transport coefficients are both arbitrarily tunable [57]. A subsequent paper on this subject will present additional simulation results for turbulent Burgers magnetohydrodynamics [58].

It remains an open problem whether the method presented here can be extended to directly recover the Burgers equation, the equations of compressible thermohydrodynamics, and the equations of magnetohydrodynamics in two and three spatial dimensions. These extensions will require using the Chapman-Enskog technique presented in this paper but for quantum models with significantly many more qubits per lattice node, say several dozen per node. Therefore efficient implementation of open quantum system models of classical turbulence in higher spatial dimensions will require a quantum computer. Fortunately, such an implementation on a future quantum computer should be straightforward because this quantum modeling method has a well-defined microscopic quantum-mechanical dynamics generated by a Hamiltonian with only local qubit-qubit interactions.

ACKNOWLEDGMENT

The author would like to thank George Vahala for useful comments on this manuscript.

[1] W. H. Zurek, Phys. Rev. D **24**, 1516 (1981).
[2] W. H. Zurek, Phys. Rev. D **26**, 1862 (1982).
[3] D. F. Walls, M. J. Collet, and G. J. Milburn, Phys. Rev. D **32**, 3208 (1985).
[4] G. J. Milburn, Phys. Rev. A **36**, 744 (1987).
[5] G. J. Milburn, Phys. Rev. A **44**, 5401 (1991).
[6] G. C. Ghirardi, A. Rimini, and T. Weber, Phys. Rev. D **34**, 470 (1986).
[7] Philip Pearle, Phys. Rev. A **39**, 2277 (1989).
[8] Gian Carlo Ghirardi, Philip Pearle, and Alberto Rimini, Phys. Rev. A **42**, 78 (1990).
[9] L. Diósi, Phys. Rev. A **40**, 1165 (1989).

[10] V. Buzek and M. Konôpka, Phys. Rev. A **58**, 1735 (1998).
[11] Carlton M. Caves, Phys. Rev. D **33**, 1643 (1986).
[12] Carlton M. Caves and G. J. Milburn, Phys. Rev. A **36**, 5543 (1987).
[13] Jeffrey Yepez, Phys. Rev. E **63**, 046702 (2001).
[14] G. V. Riazanov, Sov. Phys. JETP **6**, 1107 (1958).
[15] Richard P. Feynman and A. R. Hibbs, *Quantum Mechanics and Path Integrals* (McGraw-Hill, New York, 1965), p. 34, problem 2.6.
[16] Theodore Jacobson and L. S. Schulman, J. Phys. A **17**, 375 (1984).
[17] Iwo Bialynicki-Birula, Phys. Rev. D **49**, 6920 (1994).
[18] Sauro Succi, Comput. Phys. Commun. **146**, 317 (2002).
[19] Sauro Succi and R. Benzi, Physica D **69**, 327 (1993).
[20] Sauro Succi, Phys. Rev. E **53**, 1969 (1996).
[21] Sauro Succi, Int. J. Mod. Phys. C **9**, 1577 (1998).
[22] David A. Meyer, J. Stat. Phys. **85**, 551 (1996).
[23] David A. Meyer, Phys. Lett. A **223**, 337 (1996).
[24] David A. Meyer, Phys. Rev. E **55**, 5261 (1997).
[25] David A. Meyer, Int. J. Mod. Phys. C **8**, 717 (1997).
[26] David A. Meyer, J. Phys. A **31**, 2321 (1998).
[27] Bruce M. Boghosian and Washington Taylor IV, Int. J. Mod. Phys. C **8**, 705 (1997).
[28] Bruce M. Boghosian and Washington Taylor IV, Physica D **120**, 30 (1998).
[29] Bruce M. Boghosian and Washington Taylor IV, Phys. Rev. E **57**, 54 (1998).
[30] Jeffrey Yepez and Bruce Boghosian, Comput. Phys. Commun. **146**, 280 (2002).
[31] George Vahala, Linda Vahala, and Jeffrey Yepez, Phys. Lett. A **310**, 187 (2003).
[32] George Vahala, Linda Vahala, and Jeffrey Yepez, Proc. SPIE **5436**, 376 (2004).
[33] George Vahala, Linda Vahala, and Jeffrey Yepez, Proc. SPIE **5105**, 187 (2003).
[34] George Vahala, Linda Vahala, and Jeffrey Yepez, Philos. Trans. R. Soc. London, Ser. A **362**, 1677 (2004).
[35] Jeffrey Yepez, in *Proceedings of the Seventh International Conference on the Discrete Simulation of Fluids, Oxford* [Int. J. Mod. Phys. C **9**, 1587 (1998)].
[36] Jeffrey Yepez, Int. J. Mod. Phys. C **12**, 1285 (2001).
[37] G. P. Berman, A. A. Ezhov, D. I. Kamenev, and J. Yepez, Phys. Rev. A **66**, 012310 (2002).
[38] Jeffrey Yepez, *Quantum Computing and Quantum Communications*, Lecture Notes in Computer Science, edited by Collin P. Williams, Vol. 1509 (Springer-Verlag, Berlin, 1999) pp. 34–60.
[39] Jeffrey Yepez, J. Stat. Phys. **107**, 203 (2002).
[40] Jeffrey Yepez, e-print quant-ph/0210092.
[41] Linda Vahala, George Vahala, and Jeffrey Yepez, Phys. Lett. A **306**, 227 (2003).
[42] Jeffrey Yepez, Comput. Phys. Commun. **146**, 277 (2002).
[43] Jeffrey Yepez, Int. J. Mod. Phys. C **12**, 1273 (2001).
[44] Marco Pravia, Zhiying Chen, Jeffrey Yepez, and David G. Cory, Comput. Phys. Commun. **146**, 339 (2002).
[45] Marco Pravia, Zhiying Chen, Jeffrey Yepez, and David G. Cory, Quantum Inf. Process. **2**, 1 (2003).
[46] Zhiying Chen, Jeffrey Yepez, and David G. Cory, Phys. Rev. A **74**, 042321 (2006).
[47] R. Penrose, Proc. Cambridge Philos. Soc. **51**, 406 (1955).
[48] Bruce M. Boghosian, Jeffrey Yepez, Peter Coveney, and Alexander Wagner, Proc. R. Soc. London, Ser. A **457**, 717 (2001).
[49] Bruce Boghosian, Peter Love, and Jeffrey Yepez, Philos. Trans. R. Soc. London, Ser. A **362**, 1691 (2004).
[50] Illiya V. Karlin and Alexander N. Gorban, Phys. Rev. Lett. **81**, 1 (1998).
[51] I. V. Karlin, A. Ferrante, and H. C. Oettinger, Europhys. Lett. **47**, 182 (1999).
[52] Santosh Ansumali and Iliya V. Karlin, Phys. Rev. E **62**, 7999 (2000).
[53] Santosh Ansumali and Iliya V. Karlin, Phys. Rev. E **65**, 056312 (2002).
[54] S. Ansumali, I. V. Karlin, and H. C. Oettinger, Europhys. Lett. **63**, 798 (2003).
[55] Bruce M. Boghosian, Peter Love, and Jeffrey Yepez, Europhys. Lett. **193**, 169 (2004).
[56] R. Benzi, S. Succi, and M. Vergassola, Phys. Rep. **223**, 145 (1992).
[57] Jeffrey Yepez, George Vahala, and Linda Vahala, Proc. SPIE **5815**, 33 (2005).
[58] Jeffrey Yepez, George Vahala, and Linda Vahala (unpublished).
[59] Mehran Kardar, Giorgio Parisi, and Yi-Cheng Zhang, Phys. Rev. Lett. **56**, 889 (1986).